Supplementary Information (SI) for Nanoscale.

Supplementary information for: Rationalization of the light induced electron injection mechanism in a model 1D ZnO Nanowire-Dye complex: Insights from real-time TD-DFTB simulations.

Dalma M. Márquez,[†] Carlos R. Lien-Medrano,[*,‡] Germán J. Soldano,[¶] and Cristián G. Sánchez[*,§]

[†]*Instituto de Física Enrique Gaviola (IFEG-CONICET), Universidad Nacional de Córdoba, Córdoba 5000, Argentina.*

[‡]*Bremen Center for Computational Materials Science (BCCMS), Universität Bremen, 28359 Bremen, Germany.*

[¶]*Instituto de Investigaciones en Físico-Química de Córdoba (INFIQC-CONICET), Universidad Nacional de Córdoba, Córdoba 5000, Argentina.*

[§]*Instituto Interdisciplinario de Ciencias Básicas (ICB-CONICET), Universidad Nacional de Cuyo, Mendoza 5502, Argentina.*

E-mail: cmedrano@uni-bremen.de; csanchez@mendoza-conicet.gob.ar

DFT adsorption calculations.

Several high-symmetry adsorption sites for the dye on the nanowire were evaluated using DFT through the Quantum Espresso code.[1] The GBRV pseudopotential library, which has been optimised for precision and efficiency, was employed.[2] The energy cutoff was fixed at

50 Ry for the wave functions and 500 Ry for the charge density, with a Marzari–Vanderbilt smearing of 0.01 Ry. A Monkhorst–Pack scheme was employed to sample the Brillouin zone with 1×1×3 k-points for a 22.00×22.00×10.77 Å supercell, corresponding to the complex C_2. Relaxations were converged when forces acting on atoms were weaker than 0.02 eV/Å. The resulting geometries and relative potential energies are presented in Figure S1.

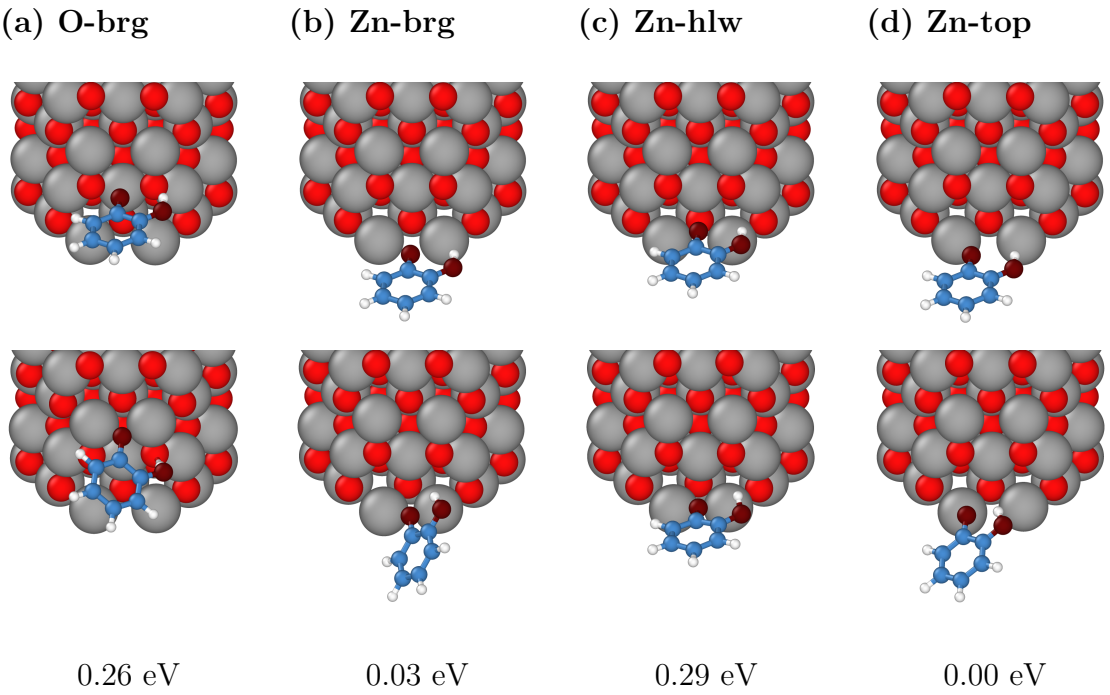

Fig. S1: Initial (top) and final (bottom) geometries of the dye relaxed at various adsorption sites. The labeling is related to the atom of the nanowire at which the dye is bonded to through its oxygen without hydrogen: oxygen-bridge (a), zinc-bridge (b), zinc-hollow (c), and zinc-top. The potential energy of the relaxed structures relative to the most stable configuration is also shown. Oxygen atoms in the dye are depicted in dark red to distinguish them from the nanowire oxygen atoms. The Zn-top is the most stable configuration, which is the one all our calculations are based on. In the case of the O-brg, the dye shifts to another adsorption site similar to a zinc-bridge.

Electronic structure calculations.

Band structure calculations for bare NWs.

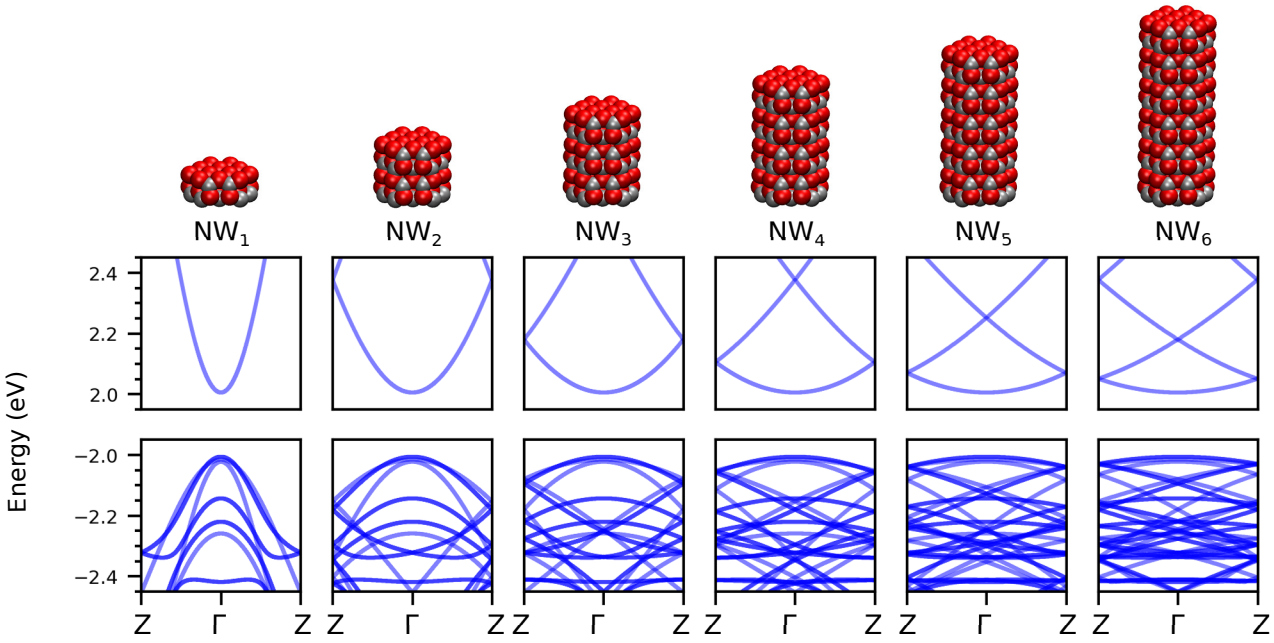

Fig. S2: Band structure for each bare NW. The unit cells employed (above) show different lengths.

Calculation of Adsorption Energies for CAT-ZnO NW complexes.

The adsorption energies for CAT-ZnO NW complexes were determined using the following equation:

$$E_{\mathrm{ad}} = E_{\mathrm{CAT+NW}} - E_{\mathrm{CAT}} - E_{\mathrm{NW}} \tag{1}$$

where $E_{\mathrm{CAT+NW}}$ is the total energy of the CAT- ZnO NW complex, E_{CAT} is the total energy of the CAT molecule, and E_{NW} is the total energy of the ZnO NW under consideration.

Representation of molecular orbitals.

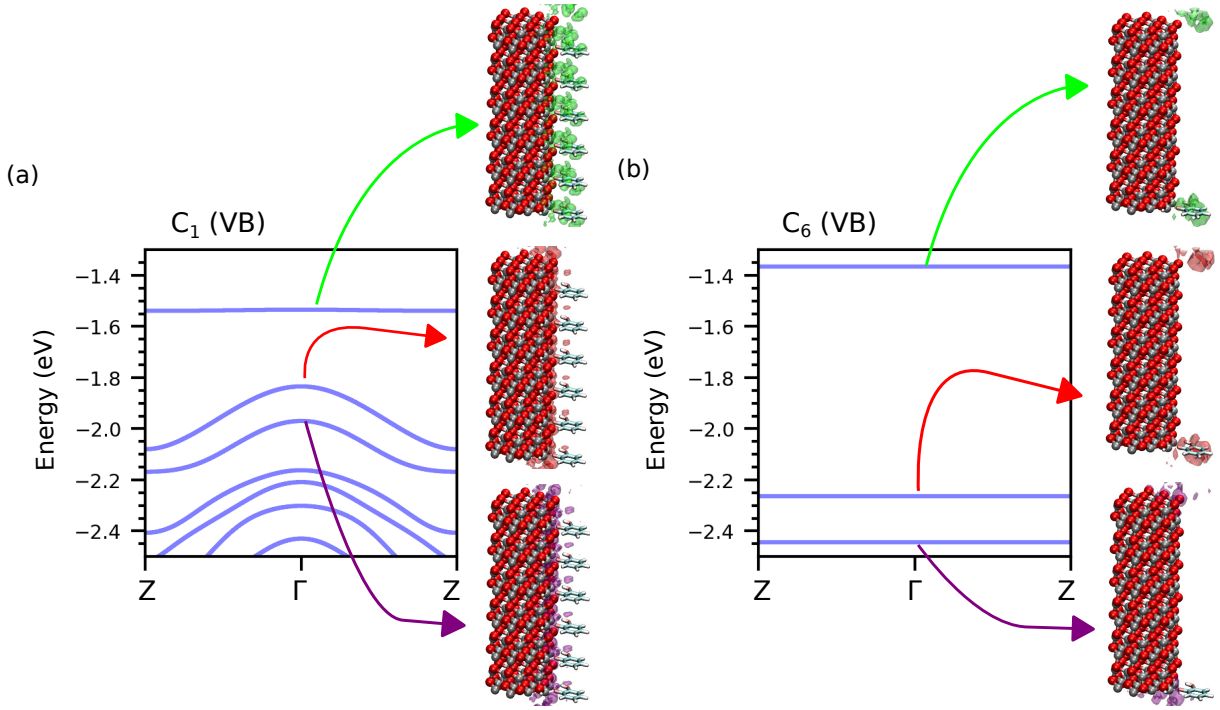

Fig. S3: Valence band structure and Γ-point molecular orbitals schematic of the lowest (a) and highest (b) covering systems (C_1 and C_6, respectively).

Fig. S3 shows the valence band and molecular orbitals of the three highest energy bands for both the C_1 and C_6 systems. It is important to note that bands with no dispersion are correlated with molecular orbitals that mainly include contributions from CAT. Conversely, bands that show dispersion are associated with NW orbitals. The dispersion of the bands is determined by the separation between CATs in adjacent unit cells.

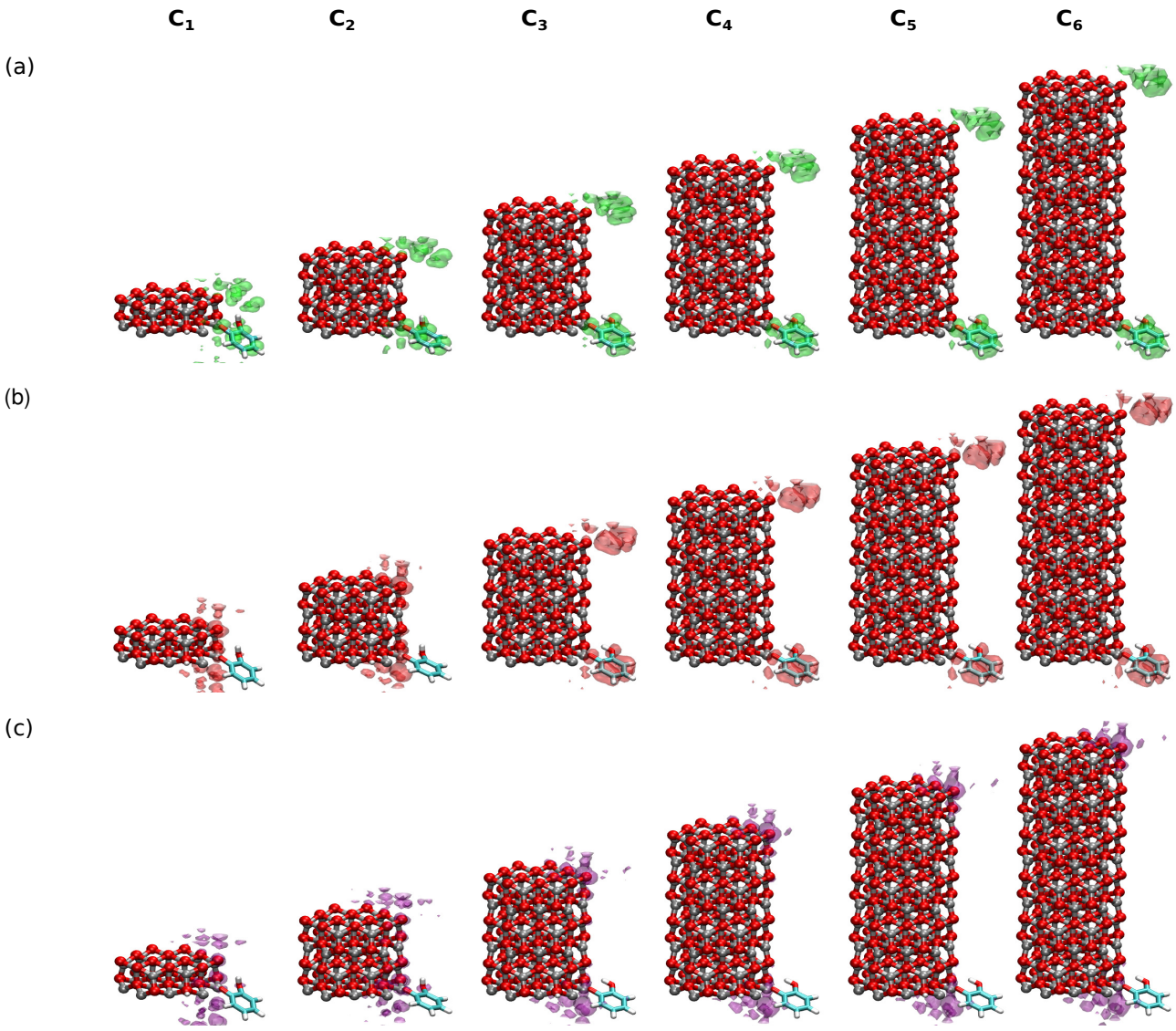

Fig. S4: Molecular orbitals representation of the most energetic bands of the valence band (at Γ point) for each complex. The edge valence band is shown in green (a), the next one in red (b) and the third one in violet (c).

Excited state calculations.

Spectra k-points convergence.

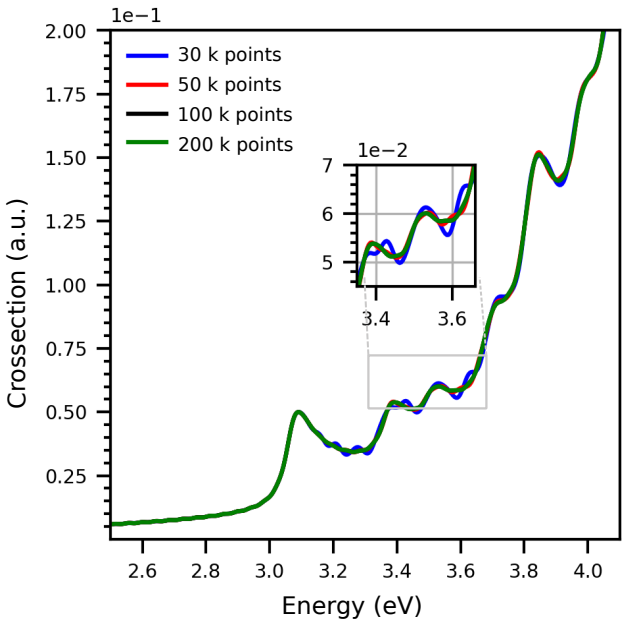

Fig. S5: Electronic spectra for the C_1 system using different numbers of k-points to sample the non-periodic direction of the first Brillouin zone. In all cases, an exponential damping decay time of 20 fs was used.

Isolated CAT spectrum.

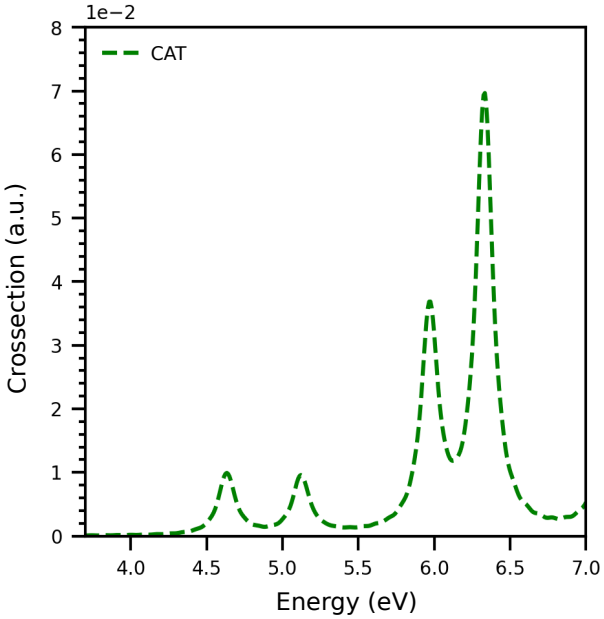

Fig. S6: Optical absorption spectrum of isolated CAT obtained theoretically with DFTB+.

Charge density difference plots

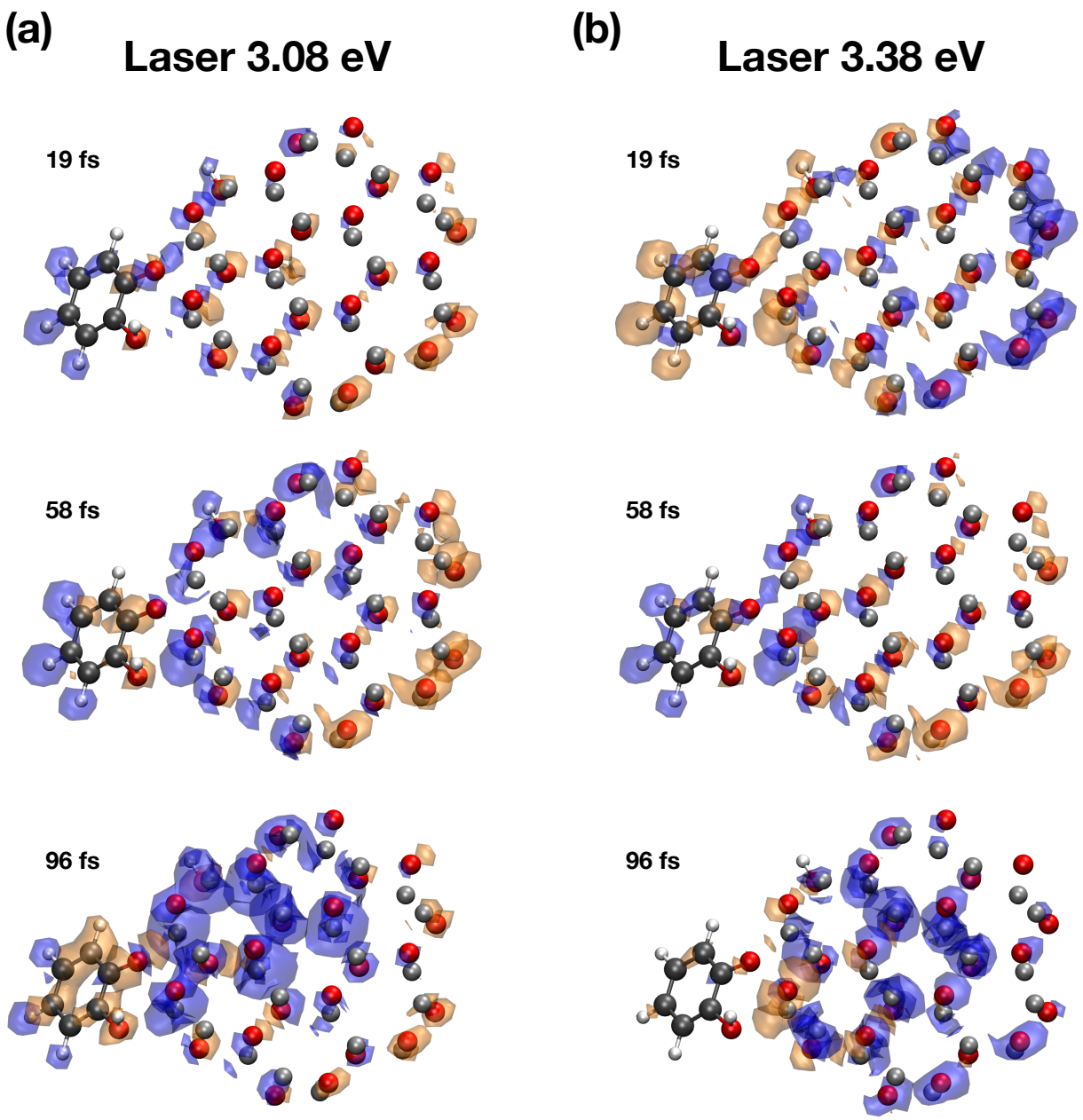

Fig. S7: Charge density difference plots for C1 at 3 snapshots during electron dynamics at (a) 3.08 eV and (b) 3.38 eV. Blue means charge accumulation and orange charge depletation. The corresponding time of the snapshots is indicated within the plot. In the case of the laser at 3.08 eV (a) there is a clear positive charge accumulation on the molecule, meanwhile an electron injection to the nanowire can be observed. In the case of the laser at 3.38 eV (b), no net charge transfer can be observed.

k-resolved dynamic band populations under photoexcitation of C_1.

In Fig. S8(a), the plot of $F(t, w)$ as a function of w (as described by equation 10 in the following section) is presented at four different times. The band structure calculation (blue) shows the temporal evolution of the populations at these four times (orange) using the analytical model proposed in this work, which is based on the Fermi golden rule (it is shown in Fig. S8(b)).

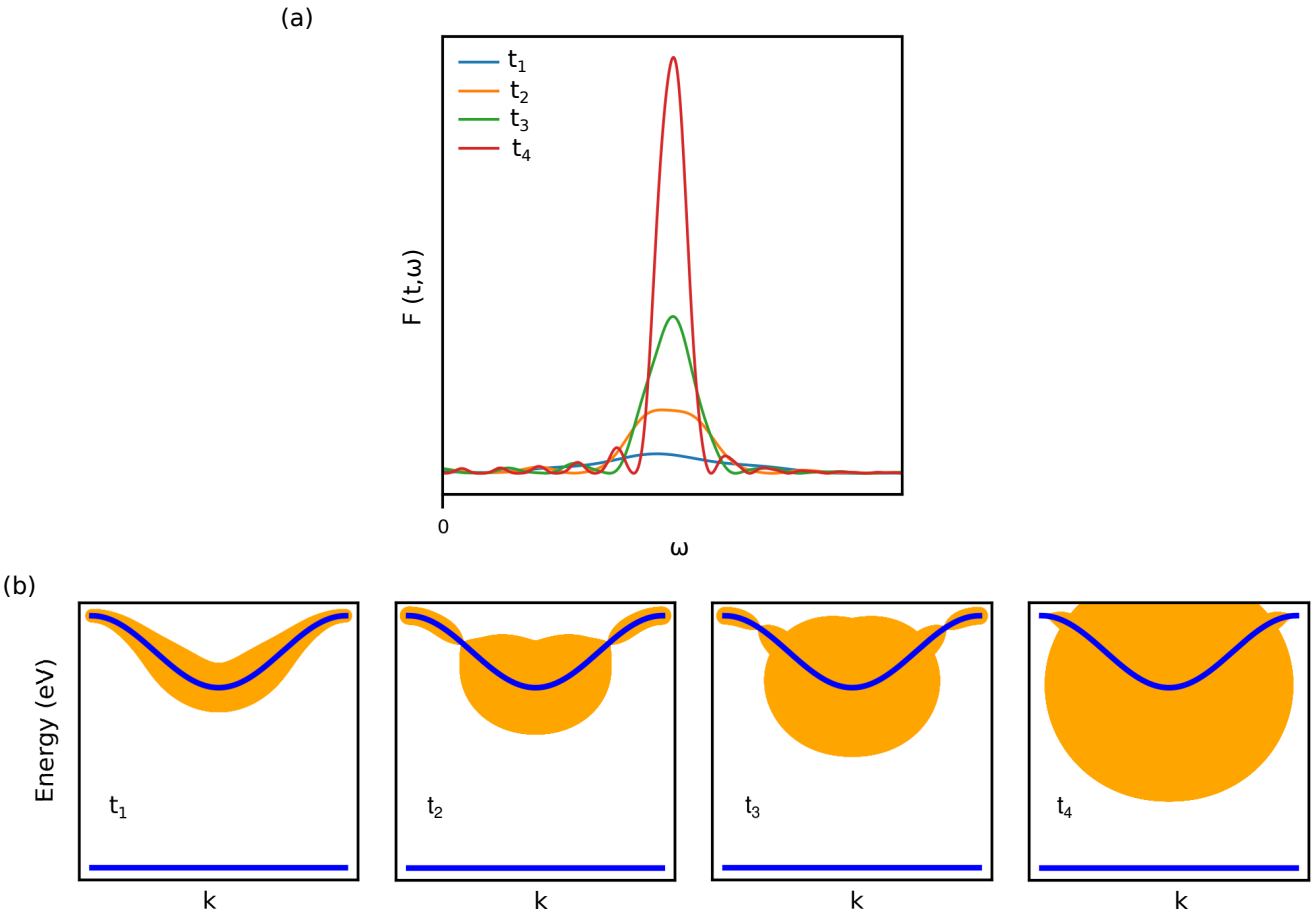

Fig. S8: (a) F(t, w) versus frequency (w) for four times where $t_1 < t_2 < t_3 < t_4$. (b) Calculations of the band structure (blue) and ΔP (orange) using the Fermi's Golden Rule.

In Fig. S9, the band electron population difference (ΔP) under excitation at energies of 3.50 eV, 3.70 eV, 3.83 eV (a), and 3.97 eV (c) is plotted for three different times: 12, 48 and 72 fs. As the irradiation energy increases, new transitions appear. Moreover, the excitations originating from the lower energy bands show a tendency to move closer to the critical point

Z while moving away from the Γ-point.

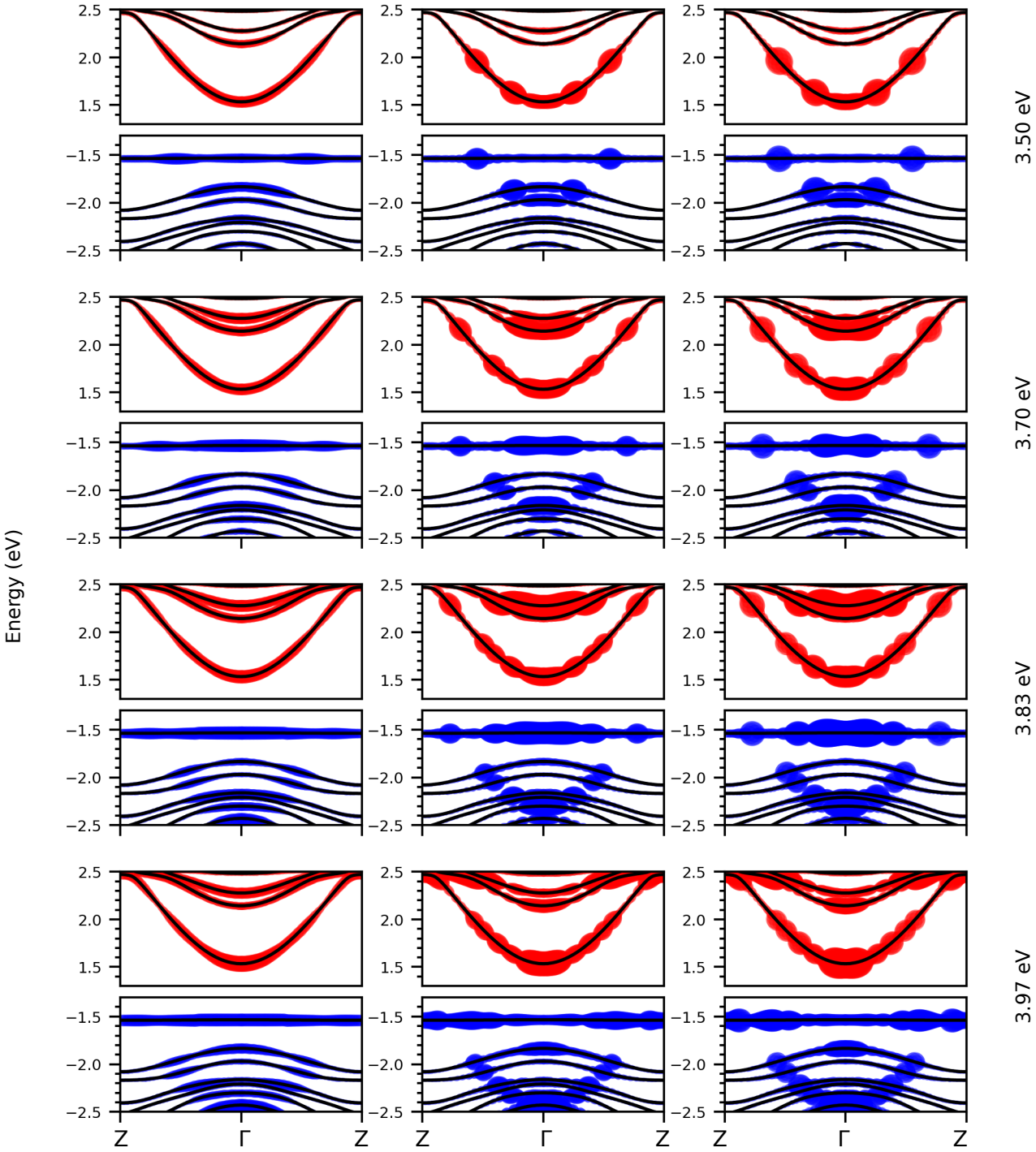

Fig. S9: Plots of the band structure and ΔP of C_1 generated by illuminating the system with laser energies of 3.50 eV, 3.70 eV, 3.83 eV and 3.97 eV at three different times: $\Delta P-$ in blue and $\Delta P+$ in red.

Derivation of Fermi's Golden Rule model.

The time evolution of electronic populations upon application of a continuous laser in the C_1 complex can be analyzed using the real-time TD-DFTB method (see Fig. 4 in the manuscript). We proposed a simple analytical model based on the Fermi Golden Rule, which allows us to understand the changes in the populations. In this case, the initial state is the valence band edge, and the final state is the conduction band edge. To capture the dynamics of the system, we use the time-dependent Schrödinger equation:

$$H|\Psi(t)\rangle = [H_0 + W(t)]|\Psi(t)\rangle = i\hbar\frac{\partial|\Psi(t)\rangle}{\partial t}, \tag{2}$$

where the Hamiltonian, denoted as H, is $H = H_0 + W(t)$. Here, H_0 is the unperturbed Hamiltonian and $W(t)$ is the time-dependent perturbation that is applied to the system. The state of the system at time t, denoted as $|\Psi\rangle$, can be expressed as a linear combination of basis functions ϕ_n:

$$|\Psi(t)\rangle = \sum_n c_n(t)|\Psi(t)\rangle = \sum_n c_n(t)|\phi_n\rangle e^{\frac{-iE_nt}{\hbar}}. \tag{3}$$

By inserting the equation 3 into 2 and projecting to ϕ_n we obtain:

$$\frac{\partial c_n(t)}{\partial t} = \frac{1}{i\hbar}\sum_k c_k(t)W_{nk}(t)e^{iw_{nk}t}, \tag{4}$$

where W_{nk} represents the perturbation matrix elements, calculated as $\langle\phi_n|W(t)|\phi_k\rangle$. Additionally, w_{nk} is $\frac{E_n - E_k}{\hbar}$. To determine the coefficients of equation 4, we make certain assumptions. First, at t = 0, we assume that all coefficients in $t = 0$ are zero, except for c_i: c_j (t = 0) = δ_{ij}. Moreover, we assume that the perturbation applied is weak and of short duration, resulting in minimal changes in the coefficients. Consequently, the equation 4 can be simplified as follows:

$$\frac{\partial c_n(t)}{\partial t} = \frac{1}{i\hbar}c_i(t)W_{ni}(t)e^{iw_{ni}t}, \tag{5}$$

for any final state the coefficient will be:

$$c_f(t) = \frac{1}{i\hbar}\int_0^t W_{fi}(t')e^{iw_{fi}t'}dt'. \tag{6}$$

The probability of finding the system in the eigenstate $|\phi_f\rangle$ (using the equation 6) is:

$$P_{if}(t) = \frac{1}{\hbar^2}\left|\int_0^t W_{fi}(t')e^{iw_{fi}t'}dt'\right|^2. \tag{7}$$

An oscillating perturbation (such as a laser) is defined as $W(t) = 2W\cos(wt) = W(e^{iwt} + e^{-iwt})$ and inserting this equation into 6 we get:

$$c_f(t) = \frac{W_{fi}}{i\hbar}\left\{\frac{e^{i(w_{fi}+w)t}-1}{i(w_{fi}+w)} + \frac{e^{i(w_{fi}-w)t}-1}{i(w_{fi}-w)}\right\}. \tag{8}$$

Introducing the function $F(t, w - w_{fi})$, the equation 7 becomes:

$$P_{if}(t) = \frac{W_{fi}^2}{\hbar^2}\left|\frac{e^{i(w_{fi}+w)t}-1}{i(w_{fi}+w)} + \frac{e^{i(w_{fi}-w)t}-1}{i(w_{fi}-w)}\right|^2 \tag{9}$$

$$= \frac{W_{fi}^2}{\hbar^2}F(t, w - w_{fi}). \tag{10}$$

When the final state is part of a continuum of states, the probability is determined by integrating the equation 10 with respect to the density of states function, denoted as DOS(E). The integration is performed by weighting each energy value with the corresponding DOS(E):

$$P(t) = \int_{E_{acc}} P_{if}(t)DOS(E)dE, \tag{11}$$

where E_{acc} represents the set of all states to which the system can transition under the influence of the perturbation. By substituting equation 10 into equation 11, we arrive at the following expression:

$$P(t) = \int_{E_{acc}} \frac{W_{fi}^2}{\hbar^2}F(t, w - w_{fi})DOS(E)dE. \tag{12}$$

Due to the narrow range of energies involved, we can treat the matrix element W_{fi} and the density of states $DOS(E)$ as constants. As a result, the probability can be expressed as an integral of the function $F(t, w - w_{fi})$:

$$P(t) = \frac{W_{fi}^2}{\hbar^2}\, DOS(E) \int_{E_{acc}} F(t, w - w_{f_i})\, dE \tag{13}$$

References

(1) Giannozzi, P.; Baroni, S.; Bonini, N.; Calandra, M.; Car, R.; Cavazzoni, C.; Ceresoli, D.; Chiarotti, G. L.; Cococcioni, M.; Dabo, I.; others QUANTUM ESPRESSO: a modular and open-source software project for quantum simulations of materials. *J. Phys.: Condens. Matter* **2009**, *21*, 395502.

(2) Garrity, K. F.; Bennett, J. W.; Rabe, K. M.; Vanderbilt, D. Pseudopotentials for high-throughput DFT calculations. *Computational Materials Science* **2014**, *81*, 446–452.